Devolatilization and Combustion of Tire Rubber and Pine Wood in a Pilot Scale Rotary Kiln

Nielsen, Anders R.; Larsen, Morten B.; Glarborg, Peter; Dam-Johansen, Kim

Published in:
Energy & Fuels

Link to article, DOI:
10.1021/ef201353t

Publication date:
2012

Document Version
Publisher's PDF, also known as Version of record

energy&fuels

Article

pubs.acs.org/EF

Devolatilization and Combustion of Tire Rubber and Pine Wood in a Pilot Scale Rotary Kiln

Anders R. Nielsen,*[,†,‡] Morten B. Larsen,[†] Peter Glarborg,[‡] and Kim Dam-Johansen[‡]

[†]FLSmidth A/S, Vigerslev Allé 77, DK-2500 Valby, Denmark

[‡]Department of Chemical Engineering, CHEC Research Centre, Technical University of Denmark (DTU), DK-2800 Lyngby, Denmark

ABSTRACT: Cement production is highly energy intensive and requires large quantities of fuels. For both economical and environmental reasons, there is an increasing tendency for utilization of alternative fuels in the cement industry, examples being tire derived fuels, waste wood, or different types of industrial waste. In this study, devolatilization and combustion of large particles of tire rubber and pine wood with equivalent diameters of 10 mm to 26 mm are investigated in a pilot scale rotary kiln able to simulate the process conditions present in the material inlet end of cement rotary kilns. Investigated temperatures varied from 700 to 1000 °C, and oxygen concentrations varied from 5% v/v O_2 to 21% v/v O_2. The devolatilization time of tire rubber and pine wood were found to mainly depend on temperature and particle size and were within 40 to 170 s. Rate limiting parameters for char oxidation of tire rubber and pine wood were found to be bulk oxygen concentration, mass transfer rate of oxygen, raw material fill degree, raw material characteristics, and temperature. Kiln rotational speed only had a minor effect on the char oxidation when the raw material bed was in a rolling motion. Initial fuel particle size also influenced the char conversion time for pine wood char but had no influence on tire char conversion time, because the tire rubber crackled into several smaller char fragments immediately after devolatilization. The char conversion times were from 40 to 480 s for tire char and from 30 to 1300 s for pine wood char, depending on the conditions. Models for devolatilization and char oxidation of tire rubber and pine wood are validated against experimental results.

INTRODUCTION

The cement industry is responsible for approximately 2% of the world's primary energy consumption.[1−3] Fuel consumption accounts for about 30−40% of the total cement clinker production costs.[4] Due to competition in the cement market, increasing fossil fuel prices, and environmental concerns, cement producers have increased the utilization of alternative fuels as a substitute for fossil fuels in order to achieve the most economic fuel mix. In this context, "alternative fuels" cover all nonfossil fuels and waste from other industries. Popular alternative fuels in the cement industry are tire-derived fuels (TDF), biomass residues, and different commercial and industrial wastes.

It is attractive to utilize coarse, solid alternative fuel particles directly in the material inlet end of cement rotary kilns in order to save expenses for shredding of the fuels to smaller particles and to increase fuel flexibility of the system. High temperatures in the rotary kiln and material retention times of several minutes provide good conditions for fuel burnout. Combustion of solid fuels in the material inlet end may, however, have negative impact on the process stability of the kiln system in the form of increased tendency for deposit build-ups. The mechanism behind formation of deposit build-ups is described elsewhere.[5] The influence of alternative fuel utilization in the material inlet end of the rotary kiln on process stability often limits how large quantities of fuel are possible to use in this way. Little information is available in the literature about combustion of large fuel particles under the conditions in the material inlet end of rotary kilns, and it is possible that a systematic investigation can optimize the utilization of alternative fuels in the material inlet end of rotary kilns. Figure 1 shows utilization of large fuel particles in the form of whole tires in the material inlet end of the rotary kiln. The raw material bed temperature is typically around 900 °C and increases toward 1450 °C in the burning zone. The gas temperature is around 1000−1200 °C in the material inlet end and may be above 2000 °C in the burner flame in the burning zone. Bulk oxygen concentration in the material inlet end is typically quite low, 2−7% v/v. Solids and gas residence times in the rotary kiln are typically 15−30 min and 5−10 s, respectively.

Devolatilization of large TDF particles have been studied by several researchers.[6−12] In addition, studies have been made with micro thermogravimetric analysis (micro-TGA) on small TDF samples to determine reaction kinetics and composition of oil, gas, and char.[13−15] Devolatilization times of cylindrical tire rubber particles with diameters from 7 to 22 mm and heights of 35 mm at 840 °C in an inert atmosphere are reported to be 75 to 300 s when increasing the particle diameter from 7.5 to 22 mm.[11] Devolatilization times of tire rubber particles with thicknesses in the range of 6−12 mm in air and in the temperature interval from 700 to 1000 °C were found to be 30−100 s depending on thickness and temperature.[12] Generally, results reported in literature about devolatilization of large TDF particles show clear tendencies for devolatilization time to increase with increasing particle size and decrease with increasing temperature and/or oxygen concentration.

Received: September 8, 2011
Revised: December 20, 2011
Published: December 20, 2011

   dx.doi.org/10.1021/ef201353t | *Energy Fuels* 2012, 26, 854−868

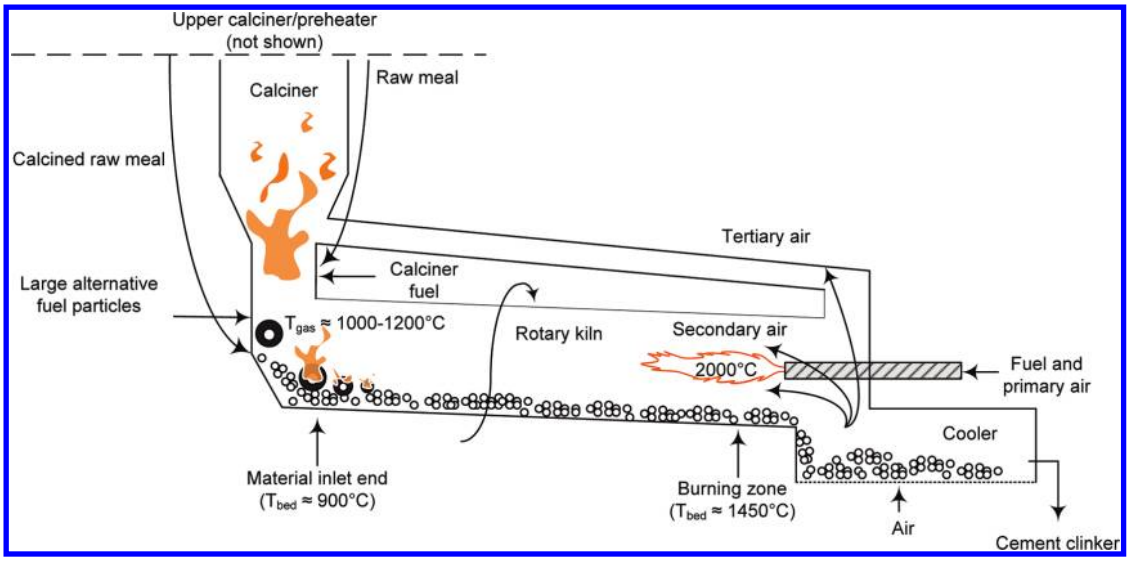

Figure 1. Utilization of large solid alternative fuel particles in the material inlet end of cement rotary kilns. Typical gas and bed temperatures shown for clarity.

Previous work about tire char combustion has been made with a few mg of tire char particles in the 100−500 μm size in thermogravimetric analyzers (TGA reactors) and drop tube reactors.[13,14,16−18] Char conversion times are reported to be well below 1 s in air and at 1200 °C for tire char with particle size of around 500 μm.[16] Oxidation time for tire char with particle size between 102 and 212 μm at 10% v/v O_2 were found to be from 9 s at 750 °C to 4 s at 850 °C.[18] Masi et al. found that a TDF char particle with a diameter of 100 μm reached full conversion after 6 s at 5% v/v O_2 and 850 °C.[17] According to Masi et al., a medium rank coal char would require 100 s to reach full conversion under the same conditions.[17] Masi et al. also compared intrinsic TDF char reactivity with the intrinsic char reactivity of refuse derived fuels (RDF) and biomass (Robinia Pseudoacacia) and found that the TDF char was most reactive.[17] Atal and Levendis also reported that tire char burned 2−4 times faster than bituminous coal char.[16] Larsen et al. concluded that the TDF chars were very reactive at temperatures of 850 °C and higher.[18] As a consequence, intraparticle kinetics were concluded to be less important because the reaction would take place at the outer particle surface. In addition, the ash layer formed on the particle surface was observed to be very porous and could easily be removed by slight mechanical interaction of the particle with tweezers. In the rotary kiln, the rotational movement of the kiln is assumed to remove the ash layer rapidly, leaving an unconverted char particle.

Devolatilization of large wood particles has also been studied by several researchers.[19−24] Winter et al. measured temperature profiles in spherical 3−20 mm diameter beech wood particles at oxygen concentrations from 0 to 21% v/v and temperatures from 700 to 950 °C. The experiments were made in a fluidized bed with silica sand as bed material. The devolatilization time of a 10 mm diameter beech wood particle at 800 °C and oxygen concentration of 10% v/v was approximately 55 s.[19] Devolatilization of nonspherical pine wood particles with equivalent diameters, d_{eff}, in the range of 10 to 45 mm and in the temperature interval of 650 to 850 °C has been investigated by de Diego et al.[21,22] The reported devolatilization times for 10 to 30 mm diameter particles were, for example, from 30 to 150 s at 850 °C. The devolatilization was reported to be only slightly affected by a change in atmosphere from air to nitrogen.[21,22] Di Blasi and Branca studied temperature profiles in cylindrical beech wood particles with lengths of 20 mm and diameters from 2 to 10 mm.[23] The experimental setup was a fluidized bed with sand as bed material and an inert atmosphere of nitrogen. Bed temperatures were from 439 to 834 °C. An empirical correlation was suggested for the devolatilization time, and the devolatilization time for a 10 mm diameter beech wood particle at 834 °C was, for example, found to be approximately 40 s.[23] Jand and Foscolo studied the pyrolysis of spherical beech wood particles with diameters from 5 to 20 mm and in the temperature interval of 560−740 °C, in a fluidized bed gasifier with sand as bed material. The devolatilization times at 740 °C were from 40 to 140 s, depending on the particle diameter.[24]

The results reported in literature about devolatilization of large wood particles are as indicated above, typically based on experiments in fluidized bed reactors with sand as bed material and at temperatures in the interval of 400−1000 °C. The wood types are either beech wood or pine wood. The general tendencies are that devolatilization times increase with increasing particle size and decrease with increasing temperatures. The effect of the atmosphere seems to be of minor importance.

Most studies with wood char combustion are made with wood chars with particle sizes in the μm range.[25−27] These studies typically use TGA experiments to obtain information about char intrinsic kinetics. Jand and Foscolo studied the char combustion of large spherical beech wood char particles with diameters from 5 to 20 mm at 740 °C and in air in a fluidized bed reactor.[24] The char oxidation times were found to be approximately 150 s for a 5 mm diameter char particle and 500 s for a 20 mm diameter char particle.

The aim of this work is to obtain quantitative data on the devolatilization and combustion of large particles of tire rubber and pine wood under conditions that resemble those in the material inlet end of rotary kilns. The purpose is to develop models for fuel conversion times in cement rotary kilns.

EXPERIMENTAL SECTION

Experimental Setup. The experiments were made in a high temperature pilot scale rotary kiln in a commercially available chamber

dx.doi.org/10.1021/ef201353t | *Energy Fuels* 2012, 26, 854−868

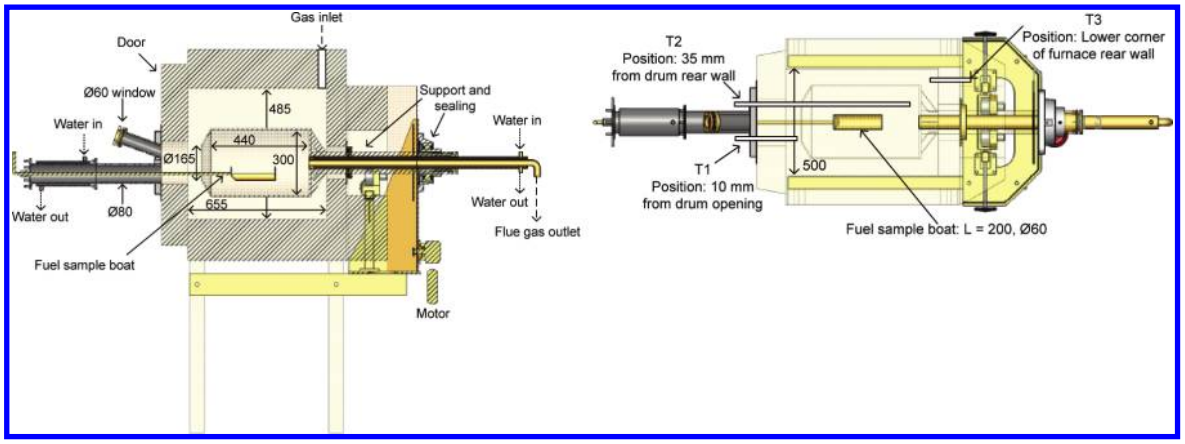

Figure 2. High temperature pilot scale rotary kiln. Left: Side view. Right: Top view.

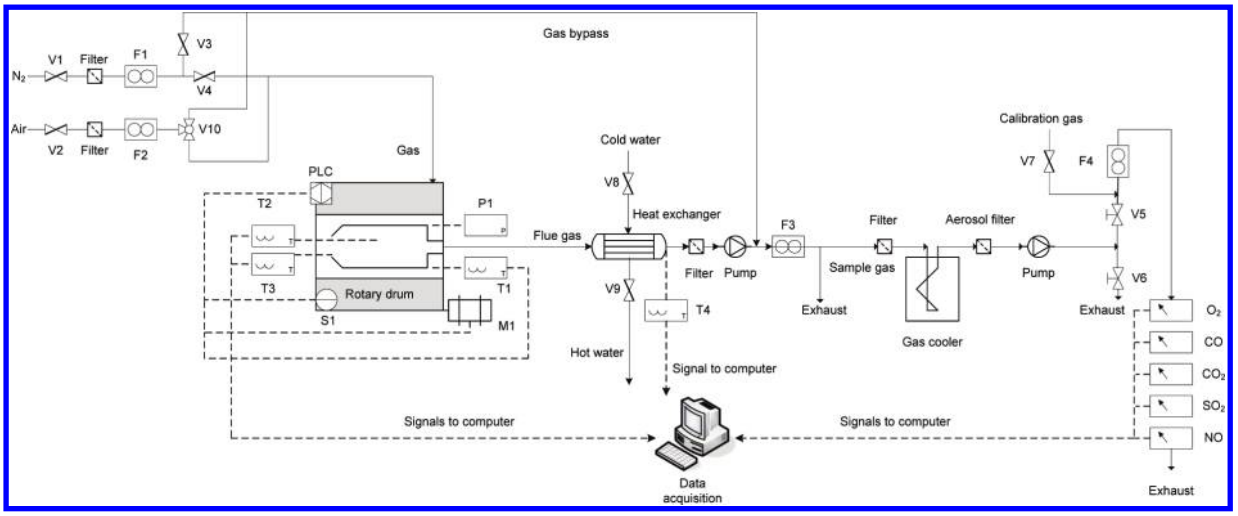

Figure 3. Sketch of the high temperature pilot scale rotary kiln experimental setup.

furnace; see Figure 2. The setup can reach an operating temperature of 1000 °C. It is electrically heated by heating elements embedded in two side walls and the bottom. The steel kiln is supported by a steel tube on rollers which passes through the rear wall. This steel tube is connected to a motor by means of a roller chain, in order to rotate the kiln. The part of the steel tube that is outside the chamber furnace is water cooled in order to protect the rollers, roller chain, and gas seals against the high temperatures.

Gas can be transported to the chamber furnace through a hole in the roof. The furnace has been designed to achieve sufficient heating of reactant gas before entering the pilot scale rotary kiln, which was also verified by temperature measurements. The gas is transported into the rotating steel kiln due to an externally placed gas pump that pumps the gas through the rotating kiln and steel tube where after the gas exits the reactor for subsequent cooling and analysis.

The chamber furnace door is equipped with a window for visual inspection, two holes for thermocouples, and a centrally placed water cooled tube for solid fuel addition. The solid fuels are placed in a sample container which can be pushed into the hot pilot scale rotary kiln or pulled out to the water cooled tube.

The experimental setup is shown in Figure 3. The gas supply can be up to 500 NL/min of air and nitrogen. The gas is transported to the pilot scale rotary kiln reactor during the experiments but may also be bypassed during calibration of flow controllers, leakage tests, etc.

The temperature is measured in three different positions in the pilot scale rotary kiln reactor: at the rear wall in the chamber furnace (T1), in the center of the pilot scale rotary kiln (T2), and at the door just in front of the pilot scale rotary kiln (T3). A pump transports the flue gas out of the pilot scale rotary kiln reactor. Before passing the pump, the flue gas is cooled in a heat exchanger and soot particles are captured in a filter. After having passed the pump, the flue gas is sent directly either to the stack or to the gas analyzers for measurement of O_2, CO, CO_2, SO_2, and NO. The fraction of the flue gas that is transported to the analyzers will pass another two filters, a gas cooler for condensation of water, and a sample gas pump before reaching the gas analyzers.

Materials and Methods. Proximate and ultimate analyses as well as lower heating values for the tested fuel samples are shown in Table 1.

Table 1. Fuel Analyses and Lower Heating Values (LHV) for Solid Fuels Used in the Experiments[a]

	proximate analysis			ultimate analysis				
	VM	FC	Ash	C	H	N	S	LHV (MJ/kg)
tire rubber	64.6	32.6	2.8	87.4	7.1	0.3	1.2	36.9
pine wood	75.3	24.5	0.2	38.9	5.2	0.1		16.2

[a]Units are in wt % as received and MJ/kg.

Tire rubber and pine wood are cut into cylindrical and rectangular shapes, respectively.

Raw materials are placed in the kiln to obtain the desired volumetric fill degree. The reactor door is closed, and the reactor is heated to the desired temperature. The kiln rotates always when the reactor is heated and keeps the raw materials in a rolling motion, with an angle

of repose of approximately 30−40°. It is the thermocouple T2 in the center of the pilot scale rotary kiln that is used to determine the temperature prior and during the experiments. The fuel sample is placed in the sample boat, and the sample boat is then positioned in the water cooled tube. The water cooled tube is closed in the end, in order to obtain a controlled atmosphere inside the pilot scale rotary kiln reactor. The gas to the reactor is adjusted to the desired flow and oxygen concentration. The temperature at T2 and oxygen concentration at the O_2 analyzer is monitored. When a stable temperature and oxygen concentration are reached, the fuel sample boat is pushed into the pilot scale rotary kiln, turned 180° and pulled out in the water cooled tube again. The fuel sample will thus drop into the preheated raw materials and immediately be heated, followed by devolatilization and char oxidation. Temperatures and flue gas compositions are continuously logged during the experiments.

An example from a typical experiment with combustion of one tire rubber cylinder is shown in Figure 4. The oxygen concentration is

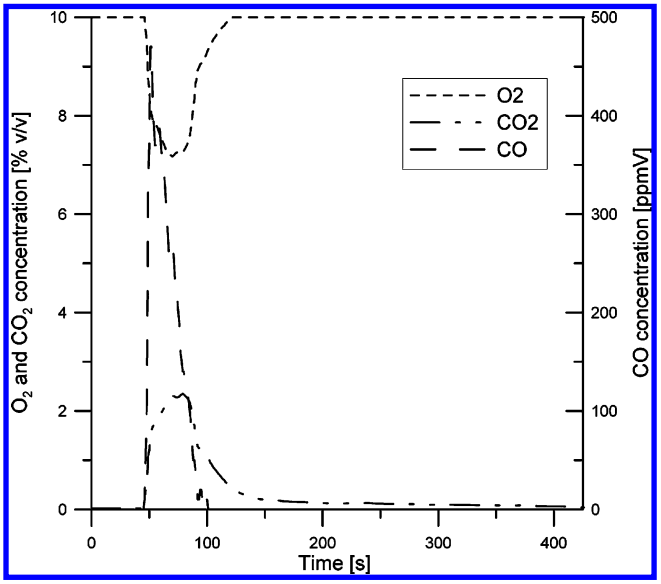

Figure 4. Example of experiment with combustion of a tire rubber cylinder. 900 °C and 10% v/v O_2. 5% volumetric kiln fill with coarse sand, 6 rpm, 100 NL/min. Particle dimensions: D = 9 mm and L = 25 mm.

observed to decrease from 10 toward 7% v/v when the devolatilization starts. At the same time, the CO concentration increases from 0 ppmV to approximately 500 ppmV, and the CO_2 concentration increases from 0 to 2.5% v/v during the devolatilization. The char oxidation is assumed to be finished when the CO_2 concentration becomes lower than 0.04% v/v. This assumption is in good agreement with the visual observations during the experiment where red-glowing char particles can be observed in the bed until the CO_2 concentration reaches values below around 0.04% v/v CO_2. Furthermore, since the experiments are made with air/nitrogen mixtures, the CO_2 concentration for experiments with pure air will never decrease below approximately 0.04% v/v, which is the CO_2 concentration in Earth's atmosphere.[28]

The degree of fuel conversion against time is derived, assuming that the fuel conversion is proportional to the carbon conversion, by integration of the concentration profiles of CO_2 and CO:[18]

$$X(t) = \frac{\int_0^t y_{CO} + y_{CO_2} dt}{\int_0^\infty y_{CO} + y_{CO_2} dt} \quad (1)$$

The repeatability of the experiments is generally found to be acceptable. Nearly all experiments were repeated at least three times to ensure the repeatability. The filters in the experimental setup have been cleaned regularly in order to avoid increases in pressure drop over the system, which were observed to affect the repeatability of individual experiments. A sensitivity analysis based on the accumulation law of uncertainties was conducted to estimate the uncertainty on the degree of fuel conversion.[29] In the estimation of the overall uncertainty, the temperature is assumed to fluctuate ±1%, the gas flow is assumed to fluctuate ±3%, and the uncertainties on each of the species CO and CO_2 are assumed to fluctuate ±1% on each species. The pressure P is assumed to be constant. The sensitivity analysis indicates an overall relative uncertainty on the estimated degree of fuel conversion in the order of ±6%.

RESULTS AND DISCUSSION

General Observations. During the experiments, it was possible to follow the devolatilization and char oxidation visually through the window. This gave a good impression of the main reaction pathways for the different fuels. For all the fuels, a flame front surrounding the fuel particles were observed almost immediately after insertion into the pilot scale rotary kiln, indicating the start of the devolatilization.

The tire rubber particles were observed to predominantly keep the particle shape under the devolatilization but with some degree of fragmentation. After the devolatilization, the tire char fragmented into several smaller char particles. The pine wood particles kept their shape during the devolatilization and, to a large extent, also during the char oxidation.

The experiments have been made with coarse sand as the raw material. This raw material was chosen because (1) it is inert and (2) it gives the desired rolling motion of the bed. It was attempted to use real cement raw material but without success due to the sticky nature of the raw material which partly resulted in a thick coating layer on the inner kiln wall and partly in clinker nodulization.

Effect of Fuel Sample Mass. The effect of fuel sample mass has been investigated with tire rubber. Figure 5 shows the

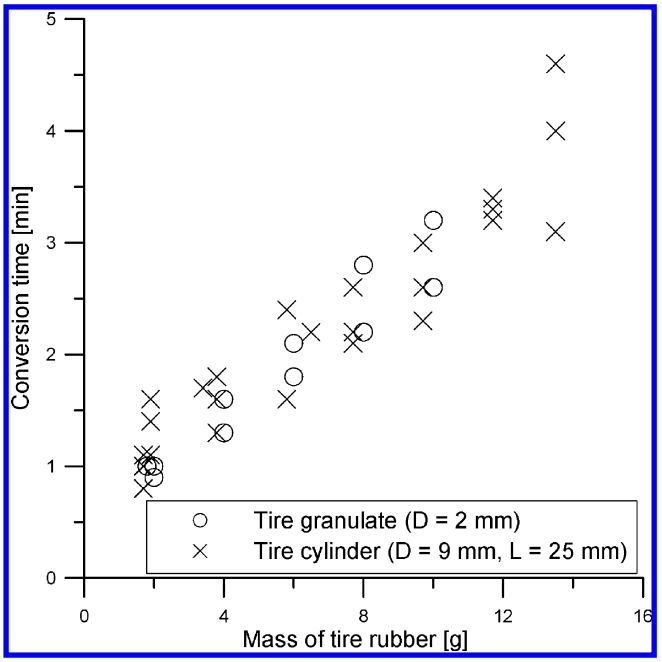

Figure 5. Conversion time versus mass for tire rubber granulate and cylinders. 10 % v/v O_2. Empty pilot scale rotary kiln, 900 °C, 6 rpm, 100 NL/min. Conversion times evaluated as 80% carbon conversion.[18]

conversion time versus mass for tire rubber cylinders with dimensions D = 9 mm and L = 25 mm and roughly spherical

dx.doi.org/10.1021/ef201353t | Energy Fuels 2012, 26, 854−868

tire rubber granulate particles with D = 2 mm. The masses are in the interval 1.8 to 15 g, and the results shown are made at 900 °C and 10% v/v O_2 and in an empty pilot scale rotary kiln. The conversion times are evaluated at 80% carbon conversion rather than at full conversion: This is to avoid the consequences of dispersion and time delay between the experimental setup and the gas analyzers which makes the time for full conversion uncertain.[18] It is observed that the conversion time increases linearly with mass for the tire cylinders as well as for the tire granulate. It is furthermore observed that there are no particular differences in conversion time for the tire cylinders and tire granulates when the total mass is the same. Thus, the initial fuel particle size of the tire rubber does not have any particular effect on the conversion time. This result is in good correspondence with the visual observation that the tire rubber rapidly cracks into several small fragments after the devolatilization, so conversion time will be a function of overall tire rubber mass rather than tire rubber particle size. The results are quite different with pine wood where the conversion time was observed to be a function of both particle size and sample mass, indicating that these fuels follow another conversion pathway than tire rubber.

Effect of Fuel Particle Size and Shape. The effect of fuel particle size has been studied with cylindrical tire rubber particles and rectangular wood particles. The rectangular wood particles are also used to study the effect of fuel particle shape. Figure 6 left shows the conversion curves for three tire rubber cylinders of different diameters (and different masses) at 900 °C and 10% v/v oxygen. The overall conversion time is observed to increase when the particle diameter (and mass) increases. It should be noted that the devolatilization time also increases when the particle diameter increases. However, on the basis of the study of fuel sample mass shown in Figure 5, it must be concluded that the increase in overall tire rubber conversion time is due to the increase in mass rather than the increase in particle diameter, since the tire char rapidly fragments into several smaller char particles.

Figure 6 right shows the carbon conversion versus time for five pine wood particles with different masses, sizes, and shapes. Four of the particles have a thickness of 10 mm while the fifth particle has a thickness of 20 mm. It is observed that the devolatilization time is approximately 1 min for the four 10 mm thick particles whereas the devolatilization time is around 2 min for the 20 mm particle; the exact devolatilization times are shown in the Model Analysis section. The char oxidation times are generally observed to increase when the mass of char increases, but it is also observed that the shape influences the char oxidation time. Three of the particles have approximately the same mass of 7 g but different char oxidation times: The longest of the 10 mm thick particles, with dimensions 120 × 15 × 10 mm, is fully combusted after approximately 11 min while the shorter, more compact particles with dimensions 60 × 30 × 10 mm and 30 × 30 × 20 require approximately 16 and 18 min for full conversion, respectively. Regarding particles with similar mass but different shapes, the reason for the difference in conversion times may be explained by the external surface area of the particles, which is largest for the particle that reaches full conversion first. Overall, the results indicate that particle thickness and external surface area have an effect on both the devolatilization time and the char combustion time.

Effect of Raw Material Bed Fill Degree. The effect of the raw material bed fill degree on the conversion time has been investigated. Figure 7 left shows the conversion time for cylindrical tire rubber particles at volumetric fill degrees of 0% (empty pilot scale rotary kiln), 5%, and 10% at 900 °C and 10% v/v oxygen. The overall carbon conversion times are observed to be highly influenced by the fill degree: In an empty pilot scale rotary kiln, the conversion time is around 100 s while it is around 200 s at 5% fill degree. For the highest fill degree of 10%, the conversion time is 600 s, significantly longer for the other two cases. It is also interesting to note that the shape of the curves are quite different, indicating that the fraction of volatile carbon and char carbon are different depending on the kiln fill degree. The reason may be differences in the heating mechanism, depending on whether the tire cylinder is buried in the bed or only exposed to the wall and freeboard gas. It has previously been reported that the heating rate of tire rubber has

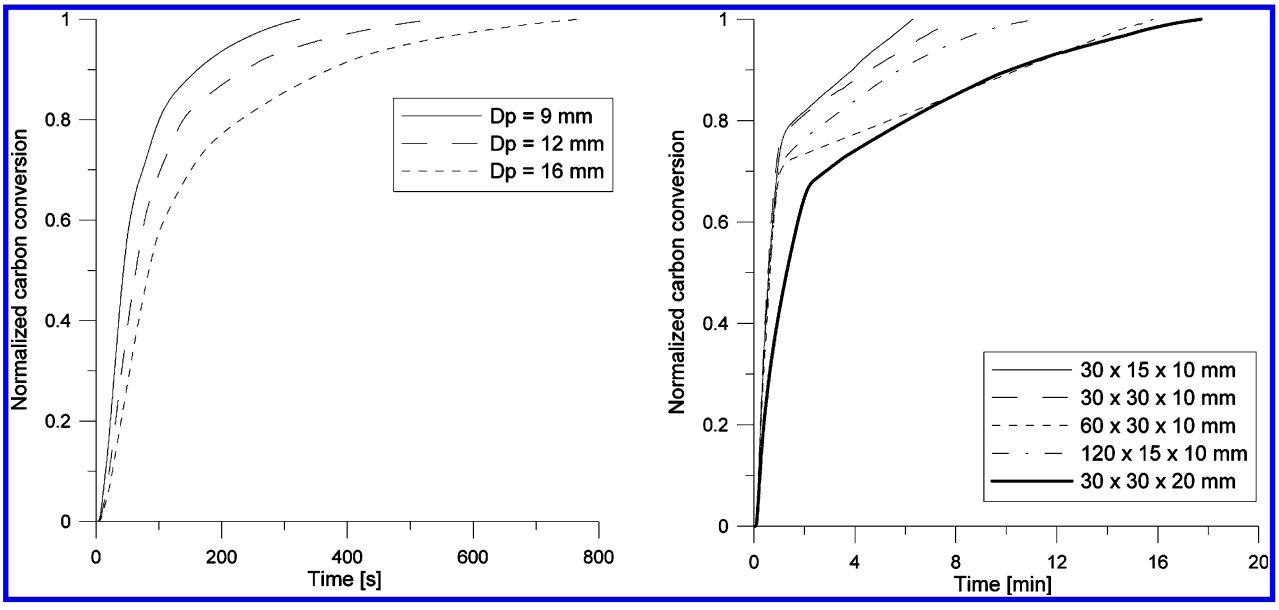

Figure 6. Left: Carbon conversion for three different tire rubber cylinders. $L_{Cylinder}$ = 25 mm. Right: Carbon conversion for pine wood particles of different sizes. T = 900 °C, 5% fill, coarse sand, 10% v/v O_2, 6 rpm, 100 NL/min.

dx.doi.org/10.1021/ef201353t | Energy Fuels 2012, 26, 854–868

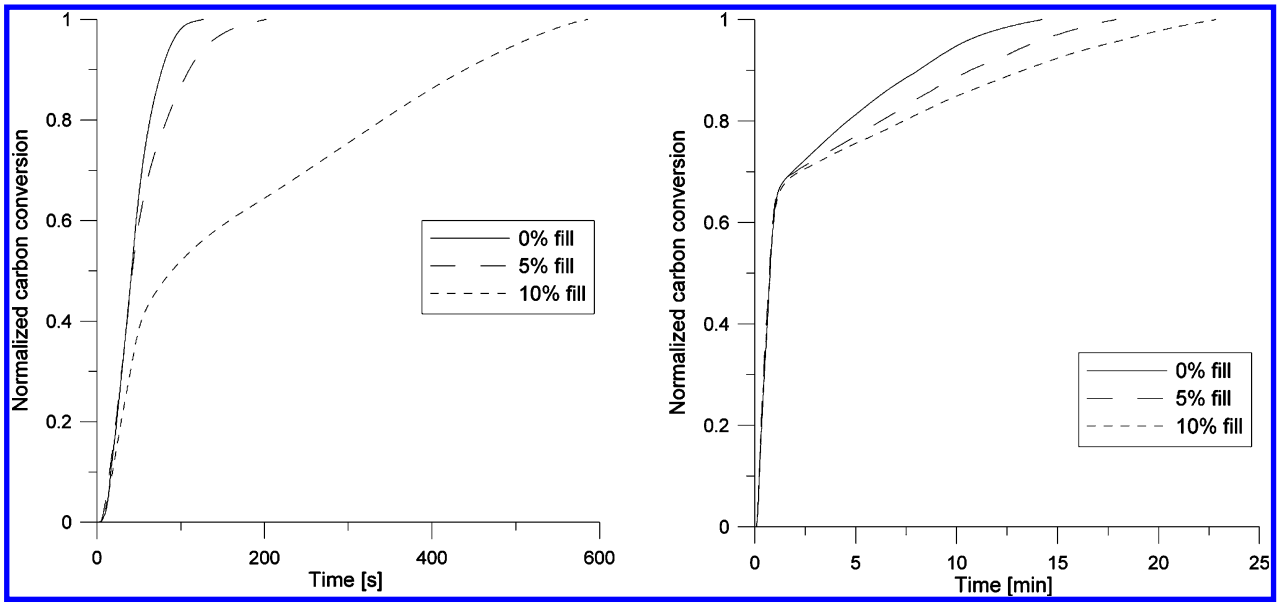

Figure 7. Carbon conversion as a function of raw material fill degree. Left: Tire rubber particle with dimensions: D = 9 mm, L = 25 mm. Right: Pine wood particle with dimensions: 60 × 30 × 10 mm. Coarse sand. T = 900 °C, 10% O_2, 6 rpm, 100 NL/min.

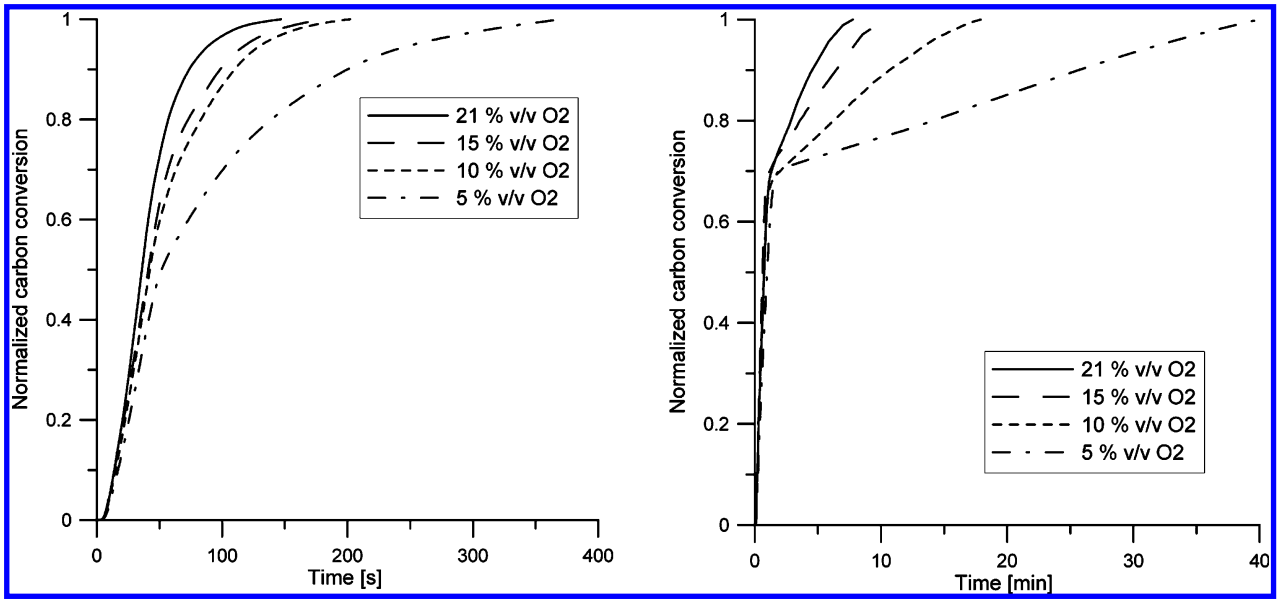

Figure 8. Carbon conversion as a function of oxygen concentration. Left: Tire rubber particle with dimensions: D = 9 mm, L = 25 mm. Right: Pine wood particle with dimensions: 60 × 30 × 10 mm. Coarse sand, 5% fill. T = 900 °C, 6 rpm, 100 NL/min.

a significant effect on the devolatilization and char combustion process.[14]

Figure 7 right shows the conversion time for a pine wood particle at fill degrees of 0% (empty pilot scale rotary kiln), 5%, and 10%. The devolatilization time is observed to be identical for the three cases while the char oxidation time increases with increasing fill degree. Thus, the raw material fill degree is of importance for the char oxidation time, which is likely to be due to diffusion limitations of oxygen to the char particle when fully or partly covered with raw materials.

Effect of Oxygen Concentration. The effect of the oxygen concentration on the conversion time has been investigated in the interval 5% v/v to 21% v/v. Figure 8 left shows the conversion time for cylindrical tire rubber particles as a function of the oxygen concentration. It is seen that the conversion time increases when the oxygen concentration decreases. The increase is approximately linear with conversion times of 140, 170, 200, and 380 s at 21, 15, 10, and 5% v/v O_2.

Figure 8 right shows the conversion time for pine wood particles as a function of the oxygen concentration. It is observed that the oxygen concentration has practically no effect on the devolatilization time but a significant effect on the char oxidation time. Full conversion is reached in less than 10 min at the highest oxygen concentrations of 21% and 15% O_2, respectively. At 10% O_2, the conversion time is 18 min, and at 5% O_2, the conversion time is 40 min. Thus, the oxygen concentration clearly has a significant effect on the conversion time of pine wood char, and the conversion time increases approximately linearly as the oxygen concentration decreases.

Effect of Rotational Speed. The effect of kiln rotational speed on the conversion time has been studied. Figure 9 left shows the conversion time for cylindrical tire rubber particles as

dx.doi.org/10.1021/ef201353t | Energy Fuels 2012, 26, 854–868

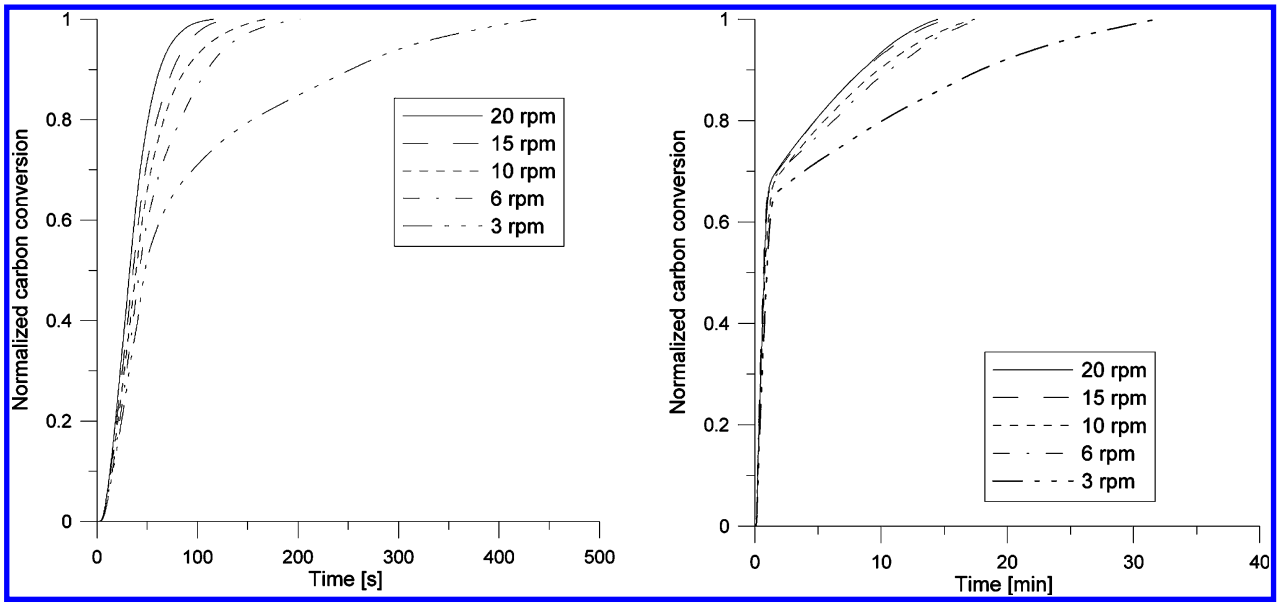

Figure 9. Carbon conversion as a function of rotational speed. Left: Tire rubber particle with dimensions: D = 9 mm, L = 25 mm. Right: Pine wood particle with dimensions: 60 × 30 × 10 mm. Coarse sand, 5% fill. T = 900 °C, 10% O_2, 100 NL/min.

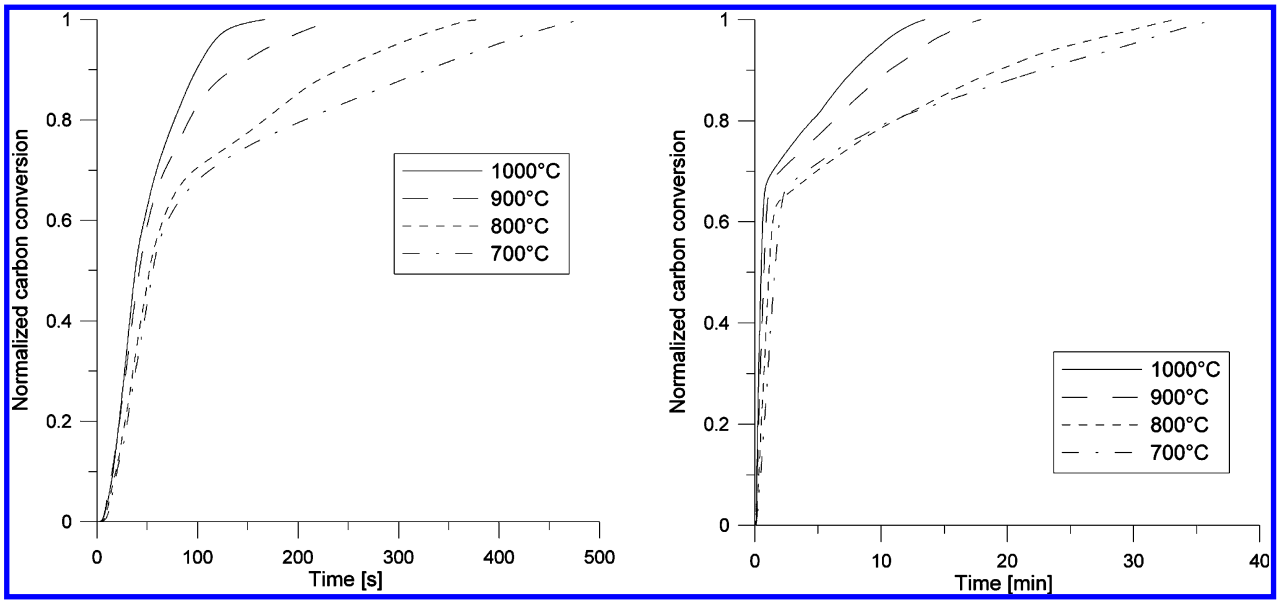

Figure 10. Carbon conversion as a function of temperature. Left: Tire particle with dimensions: D = 9 mm, L = 25 mm. Right: Pine wood particle with dimensions: 60 × 30 × 10 mm. Coarse sand, 5% fill. 6 rpm, 10% O_2, 100 NL/min.

a function of rotational speed in a bed with 5% fill degree at 900 °C and 10% v/v O_2. It is observed that the conversion time increases when the rotational speed decreases. The conversion time is, e.g., 100 s at 20 rpm and 200 s at 6 rpm, a factor 2 in difference. The conversion time increases dramatically to 440 s at the lowest rotational speed of 3 rpm. The reason is likely to be a change in bed behavior, which could also be observed visually: The bed motion is slumping at 3 rpm while it is rolling at 6 rpm and higher rotational speeds. This difference in bed motion affects the mixing process and thus the conversion time of the fuel particles. It is also possible that the fuel particle breakdown is more significant at higher rotational speeds due to stronger forces acting on the fuel particles.

Figure 9 right shows the conversion time for pine wood particles as a function of rotational speed in a bed with 5% fill degree at 900 °C and 10% v/v O_2. It is observed that there is no difference for the devolatilization time. For the char oxidation, the conversion time increases slightly when the rotational speed is decreased in the interval of 20 to 6 rpm. However, when the rotational speed is lowered to 3 rpm, the conversion time is increased significantly (33 min relative to 17 min at 6 rpm). This large effect at the lowest rotational speed is due to a change in bed behavior, from rolling to slumping.

Effect of Temperature. The effect of temperature on the conversion time has been investigated for the temperatures 700 °C, 800 °C, 900 °C, and 1000 °C. Figure 10 left shows the conversion time of tire rubber as a function of temperature. It is observed that both the devolatilization time and the char oxidation time decreases when the temperature increases. The conversion time at 1000 °C is observed to be around 160 s, while it is 490 s at 700 °C.

dx.doi.org/10.1021/ef201353t | *Energy Fuels* 2012, 26, 854–868

Figure 10 right shows the conversion time for pine wood particles as a function of temperature in the temperature interval of 700 °C to 1000 °C. Both the devolatilization time and the char oxidation time increases when the temperature decreases. However, the time difference for the char oxidation at 700 °C and 800 °C is quite small, 0 to 1 min, whereas the time is significantly shorter at 900 °C and 1000 °C.

Conclusions on Experimental Parameter Study. A parameter study has been conducted for tire rubber and pine wood. The main findings were:

For pine wood, fuel mass, particle thickness, and external surface area are important for the conversion time, both regarding devolatilization and char oxidation. For tire rubber, however, the tire char rapidly fragments into smaller particles. Consequently, the initial dimensions of the tire rubber are of little importance for the tire char conversion time. For the char oxidation part of tire rubber and pine wood, the parameters char mass, oxygen concentration, temperature, and raw material fill degree are all important parameters, but also rotational speed was observed to have an effect on the conversion time.

MODEL ANALYSIS

This section seeks to develop and verify mathematical models for devolatilization and char oxidation of selected alternative fuels. The models are to be used under conditions similar to those in the material inlet end of cement rotary kilns.

Model for Devolatilization. The heat up of a large, spherical particle may be derived by solving the unsteady heat transfer differential equation:[30,31]

$$\frac{\partial T_p}{\partial t} = \frac{1}{r^2}\frac{\partial}{\partial r}\left(r^2 \frac{k_p}{\rho_p C_p}\frac{\partial T_p}{\partial r}\right) \tag{2}$$

with the following boundary and initial conditions:

$$k_p\frac{\partial T_p}{\partial r} = Yh_{Cond}(T_b - T_p) + (1 - Y)$$
$$(h_{Conv}(T_g - T_p) + \sigma\varepsilon_p(\varepsilon_g {T_g}^4 - \alpha_g {T_p}^4)$$
$$+ \sigma\varepsilon_p(\varepsilon_w {T_w}^4 - \alpha_w {T_p}^4)) \quad \text{for} r = R \tag{3}$$

$$\frac{\partial T_p}{\partial r} = 0 \quad \text{for} r = 0 \tag{4}$$

where R is the initial radius of the particle, k_p is the thermal conductivity of the particle, ρ_p is the virgin fuel density, and C_p is the specific solid heat capacity. h_{Cond} and h_{Conv} are the heat transfer coefficients for conduction and convection, respectively. T_p, T_b, T_g, and T_w are temperatures of particle, bed, bulk gas, and inner kiln walls, respectively. Y is the dimensionless distribution of fuels in the bed, which is 1 if the fuel particles are fully covered by raw materials and 0 if the fuel particles are fully exposed to the gas phase. Equation 3 expresses that all heat transferred to the surface of the particle is conducted into the particle, and eq 4 expresses that the gradient at the particle center is zero due to symmetry. Equation 3 must be solved numerically. However, if radiation is neglected, an analytical solution can be found.[31]

$$\frac{T_a - T_p}{T_a - T_{p,0}} = 2\sum_{i=1}^{\infty}\frac{\sin\beta_i - \beta_i\cos\beta_i}{\beta_i - \sin\beta_i\cos\beta_i}\left[\frac{\sin\left[\beta_i\frac{r_p}{r_{p,0}}\right]}{\left[\beta_i\frac{r_p}{r_{p,0}}\right]}\right]$$
$$e^{-(\beta_i^2\alpha t/{r_{p,0}}^2)} \tag{5}$$

where T_a is the mean average temperature surrounding the particle. T_a may be estimated as $T_a = Y \cdot T_b + (1 - Y) \cdot T_g$. α is the thermal diffusivity, $\alpha = k_p/(\rho_p\ C_p)$.

The β_i's are the positive solutions to the equation:

$$\beta\cdot\cos\beta = (1 - Bi)\cdot\sin\beta \tag{6}$$

where Bi is the Biot number. An efficient heat transfer coefficient, h_{eff}, is used to calculate Bi, where $h_{eff} = Y \cdot h_{Cond} + (1 - Y) \cdot (h_{Conv} + h_{rad})$ and $h_{rad} = \varepsilon_g\sigma \cdot ({T_g}^2 + {T_p}^2) \cdot (T_g + T_p)$.[32]

The time, τ_{devol}, required for complete devolatilization corresponds to the time needed for the fuel particle center to reach the upper devolatilization temperature, T_{Vol2}. This time is determined from eq 5 using $T_p(0, t) = T_{Vol2}$.[33] However, eq 5 should only be used to determine the devolatilization time for an initially dry particle, since the equation does not take the particle moisture content into consideration. The moisture content of a fuel particle may influence the devolatilization time considerably.[21,22,31,33]

Validation of Devolatilization Model. If the temperature required for complete devolatilization, T_{Vol2}, is known, e.g., from TGA measurements reported in the literature, eq 5 may be used to determine the time required for full devolatilization. Table 2 shows the temperatures for initial and final devolatilization temperatures for the fuels tire rubber and pine wood.

Table 2. Temperatures for Initial and Final Devolatilization of Tire Rubber and Pine Wood

fuel	T_{Vol1} [K]	T_{Vol2} [K]	reference
tire rubber	523	773	12
pine wood	473	773	34

Experiments with nonspherical tire rubber and pine wood particles of different size and shapes have been conducted to study the devolatilization time. Since the model assumes that the fuel particles are spherical, it is required to represent the nonspherical fuel particles as spherical particles of diameter, d_{eff}, characterized by the nonspherical and spherical particles having the same total surface area:[35]

$$d_{eff} = \theta\cdot d_{sph} \tag{7}$$

where d_{sph} is the equivalent spherical diameter, defined as the diameter of a sphere with the same volume as the particle. θ is the sphericity defined as:

$$\theta = \left(\frac{\text{Surface of sphere}}{\text{Surface of particle}}\right)_{\text{of same volume}} \tag{8}$$

The experimentally found devolatilization times are determined by means of the normalized carbon conversion curves for the fuels. Figure 11 shows an example with pine wood, where the devolatilization time is observed to begin at

dx.doi.org/10.1021/ef201353t | Energy Fuels 2012, 26, 854–868

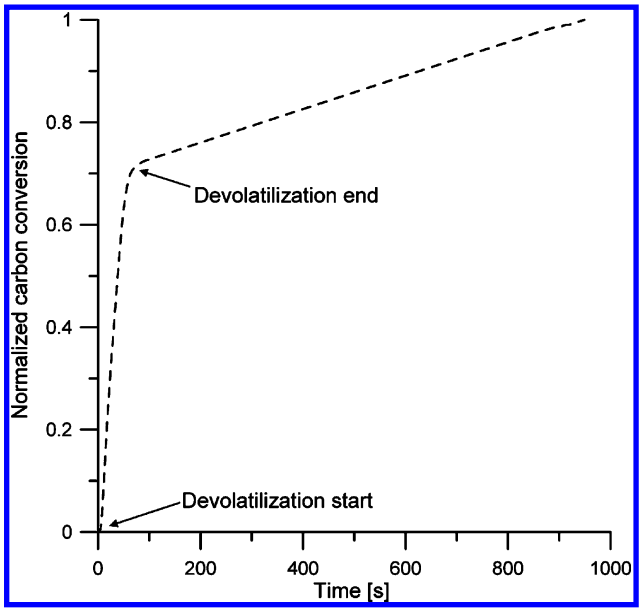

Figure 11. Determination of devolatilization time for a pine wood particle at 900 °C and 10% v/v O_2. 5% volumetric fill, coarse sand, 100 NL/min, 6 rpm. Particle dimensions: 60 × 30 × 10 mm (7.0 g).

time 0 s and end at time 80 s. The devolatilization ends when the slope of the conversion curve is observed to decrease significantly, indicating the start of the slower char oxidation.

Devolatilization of Tire Rubber. A comparison between experimental values and values predicted by the model for tire rubber is shown in Figure 12. Values used in the model are summarized in Table 3.

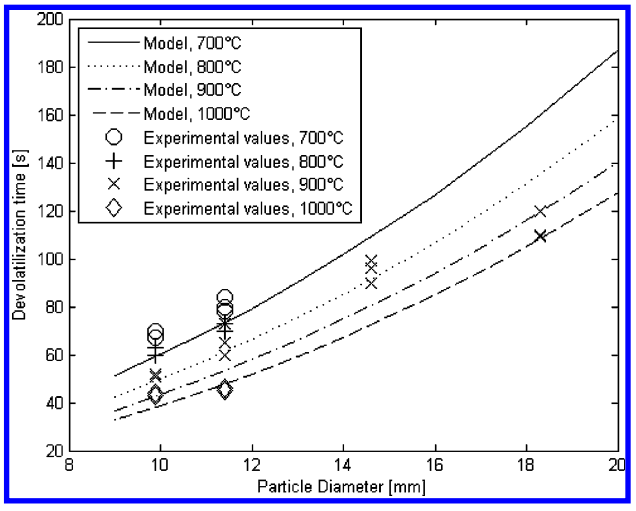

Figure 12. Comparison of tire rubber devolatilization time predicted by the model and by experimentally found values. 10% O_2. 5% volumetric fill degree in pilot scale rotary kiln. Y = 0.2. $\alpha = 1.25 \cdot 10^{-7}$ m^2/s.

In the model, the fraction of the fuel particle surface that is covered by raw materials, Y, is 0.2. This fraction was chosen on the basis of visual observations during the experiments, where the cylindrical tire rubber particle was observed to be free of the raw material bed during most of the devolatilization. The experimental values were obtained for four different tire rubber particle diameters from 10 mm to 18.5 mm and at 900 °C. The two smallest tire rubber particles were also studied at 700 °C, 800 °C, and 1000 °C. The model is in acceptable agreement with the experimental values, which were found to have devolatilization times from approximately 40 to 120 s, depending on temperature and tire rubber particle size. The model generally overestimates the effect of temperature compared to the experimental findings: For the two smallest fuel particles, the difference in experimentally found devolatilization times were smaller than that predicted by the model.

Table 3. Fuel Specific Data Used in the Devolatilization Models

property	TDF	pine wood	references
specific heat capacity, C_p, [J/(kg · K)]	2000	1500	11
			36
initial particle density, ρ_p, [kg/m^3]	1150	690	8
			36
k_p, virgin fuel thermal conductivity, [W/(m · K)]	0.3	0.2	37
			36
conductive heat transfer coefficient, h_{CBP}, [W/(m^2 · K)]	250	250	38
convective heat transfer coefficient, h_{CBP}, [W/(m^2 · K)]	150	150	39

Chinyama and Lockwood studied the devolatilization times of tire rubber particles with thicknesses in the range of 6−12 mm and in the temperature interval from 700 to 1000 °C.[12] The devolatilization times were found to be 30−100 s, depending on thickness and temperature, which were typically 20 s longer than the values found in this study for the same particle sizes and temperatures. This difference in time may be due to different heat transfer mechanisms at the two experimental conditions: In the experiments conducted by Chinyama and Lockwood, heat transfer to the tire rubber particles were exclusively by convection and radiation, whereas heat transfer in this study was also partly by conduction from the raw materials and kiln wall. Another reason may be the mechanical influence from the pilot scale rotary kiln in this study, which is likely to increase fragmentation of the fuel particle during devolatilization; in fact, the tire rubber particles were observed to fragment a little during the experiments, thereby leading to smaller fuel particle sizes.

Larsen et al. also studied the devolatilization of cylindrical tire rubber particles with diameters from 7 to 22 mm and heights of 35 mm at temperatures up to 840 °C in an inert atmosphere.[11] The reported devolatilization times at 840 °C were 75 to 300 s when increasing the particle diameter from 7.5 to 22 mm. These devolatilization times are approximately twice as long as indicated by the results from this study. The reason for the deviations may again be differences in the heat transfer mechanisms due to different experimental conditions as well as the mechanical influence in this study. In addition, the experiments conducted by Larsen et al. were made under an inert atmosphere while the present study was made under oxidizing conditions which are likely to have accelerated the devolatilization.

Devolatilization of Pine Wood. A comparison between experimentally found values and values predicted by the model for pine wood is shown in Figure 13. Values used in the model can be found in Table 3. The experimental values were obtained for five different pine wood particle diameters from 12 mm to 26 mm and at 900 °C. The pine wood particles of diameters 15 mm and 20 mm were also studied at 700 °C, 800 °C,

dx.doi.org/10.1021/ef201353t | Energy Fuels 2012, 26, 854−868

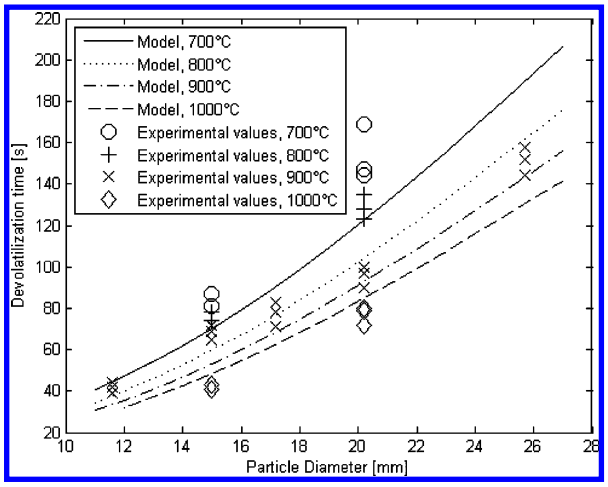

Figure 13. Comparison of pine wood devolatilization time predicted by the model and by experimentally found values. 10% O_2, 5% volumetric fill degree in kiln. $Y = 0.2$. $\alpha = 1.9 \cdot 10^{-7}$ m^2/s.

and 1000 °C. The model is observed to be in acceptable agreement with the experimental values, which were found to have devolatilization times from approximately 40−170 s, depending on temperature and particle size. However, the experiments conducted at 700 °C and 800 °C are generally 20−30 s longer than the devolatilization times predicted by the model, and in one case, with a particle diameter of 20 mm and at 700 °C, the deviation is 50 s.

Devolatilization of nonspherical pine wood particles with equivalent diameters, d_{eff}, in the range of 10 mm to 45 mm and in the temperature interval of 650 °C to 850 °C has been investigated by de Diego et al.[21,22] The reported devolatilization times were in good correspondence with the values found in the present study. For example, at 850 °C, the devolatilization times for 10 mm to 30 mm diameter particles were reported to be from 30 s to 150 s, whereas the results from this study indicates devolatilization times from 25 s to 180 s at 850 °C. These minor differences in devolatilization times may be due to different characteristics of the pine wood used in the experiments. The found devolatilization times for pine wood are also in relatively good consistency with devolatilization times for beech wood particles of similar size as reported by Di Blasi and Branca[23] and Jand and Foscolo;[24] see the literature study in the Introduction.

Model for Char Combustion. The aim of this section is to derive a model for char conversion in the pilot scale rotary kiln, including the main rate limiting parameters for char conversion. The char combustion model will be validated against experimental results. The model may be modified into a realistic char conversion model for the material inlet end of industrial rotary kilns. The char conversion model may be used in combination with models for drying and devolatilization of virgin fuel particles, or it may stand alone to simulate the fate of char particles dropping from calciners through the kiln riser duct and into the material inlet end of rotary kilns.

Figure 14 shows a rotary kiln where char particles are buried in the raw material bed. The bulk oxygen volume fraction is denoted $y_{O2,\infty}$, and the oxygen volume fraction at the bed surface is called $y_{O2,surf}$. The oxygen volume fraction at the char particle surface is called $y_{O2,part}$. The mixing of large particles into a bed of smaller particles has previously been shown to be a fast process, typically taking only a few bed revolutions.[40]

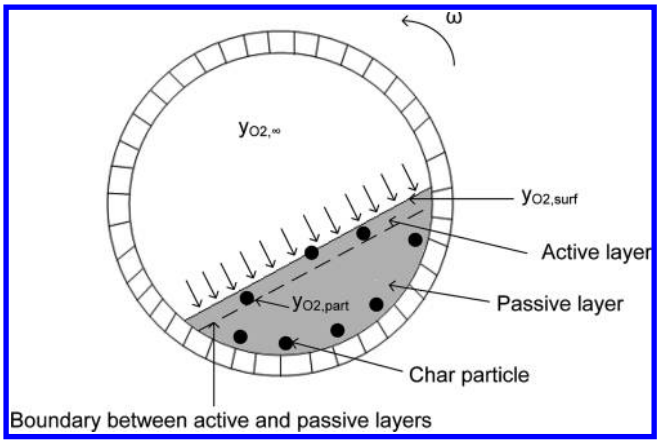

Figure 14. Oxygen mass transfer to char particles in a bed of cement raw materials in a rotary kiln.

In a cement rotary kiln, it may be assumed that mass transfer of oxygen into the active layer is fast while oxygen mass transfer into the passive layer takes place by a relatively slow diffusion; see Figure 14. Since the char particles will continuously be transported through the active and passive layers, respectively, it may be assumed that char oxidation primarily takes place when the char particles are present in the active layer.

With the above-mentioned considerations in mind, a model for char oxidation applicable for the conditions in the material inlet end of a rotary kiln should include the following: (1) external mass transfer of oxygen to bed surface, (2) mass transfer of oxygen through the active layer, (3) diffusion of oxygen into the char particle, and (4) chemical reaction of char and oxygen.

The external mass transfer of oxygen to the bed surface can be written as the mass transfer coefficient k_g multiplied by the driving force:[41]

$$r = k_g \cdot \frac{P}{RT_g} \cdot (y_{O_2,\infty} - y_{O_2,surf}) \left[\frac{\text{mol } O_2}{m^2 \cdot s}\right] \quad (9)$$

where k_g is found from a Sherwood correlation. For the pilot scale rotary kiln, where the gas flow is in the laminar regime, the following correlation is used[42]

$$Sh = \frac{k_g L}{D_{O_2}} = 0.646 Re^{1/2} Sc^{1/3} \quad (10)$$

where Re is calculated from the pilot scale rotary kiln length, L. This correlation is valid for laminar flow over a flat plate, which is roughly similar to the situation with gas flow above the bed surface.

In case of a pilot scale rotary kiln without raw materials and few fuel particles, the mass transfer coefficient may be found from a Sherwood correlation for flow past single spheres:[42]

$$Sh = \frac{k_g \cdot d_p}{D_{O_2}} = 2 + 0.6 \cdot Re_{d_p}^{1/2} \cdot Sc^{1/3}$$
$$2 \le Re_{d_p} \le 800,\ 0.6 \le Sc \le 2.5 \quad (11)$$

The mass transfer of oxygen from the bed surface into the active layer can be written as the mass transfer coefficient in the active layer, k_{AL}, multiplied by the driving force and the probability that the char particles are in the active layer, P_{AL}, at

dx.doi.org/10.1021/ef201353t | Energy Fuels 2012, 26, 854−868

any given time:

$$r = P_{AL} \cdot k_{AL} \cdot \frac{P}{RT_b} \cdot (y_{O_2,surf} - y_{O_2,part\ surf}) \left[\frac{mol\ O_2}{m^2 \cdot s}\right] \quad (12)$$

The probability for the char particles to be in the active layer may be estimated by the experimentally determined correlation suggestion by eq 13, which provides a correlation for the percentage of visible fuel particles at the bed surface:[40]

$$P_{AL} = \frac{1}{\theta^{1.5}} \cdot \frac{V_{fuel}}{V_{fuel} + \frac{\pi}{4} D^2 L F^{1.2}} \cdot Fr^{-0.09} \cdot \left(\frac{\rho_{raw\ material}}{\rho_{fuel}}\right)^{0.77} \cdot 100\% \quad (13)$$

This correlation may be used since the active layer thickness is quite small, and it therefore may be assumed that the number of fuel particles in the active layer is practically the same as the number of fuel particles that are visible above the bed surface. A bulk density of 1200 kg/m^3 is used for the raw material. The dimensionless Froude number is defined as:

$$Fr = \frac{\left(\frac{2\pi\omega}{60}\right)^2 R}{9.81\ m/s^2} \quad (14)$$

The mass transfer coefficient in the active layer, k_{AL}, has been determined by Heydenrych:[43]

$$k_{AL} = \sqrt{D_{O_2,eff} \frac{6(1-\varepsilon) \cdot Sh \cdot D_{O_2}}{d_p^{\ 2}}}, \quad Sh = 3.8 \quad (15)$$

where $D_{O2,\ eff}$ is the effective diffusion coefficient of oxygen:

$$D_{O_2,eff} = \frac{\varepsilon}{\tau} D_{O_2} \quad (16)$$

D_{O_2} is the diffusion coefficient for oxygen in air, τ is the bed tortuosity, and ε is the bed porosity or void fraction available for gas flow. Dias et al. found that the tortuosity, τ, of a mixed bed of granular particles could be described as $\tau = 1/\varepsilon^n$, where n depends on the particle packing but usually is in the range of 0.4−0.5.[44]

The rate of oxygen diffusion into the char particle may be estimated by the expression:

$$r = \frac{D_{O_2,part}}{r_p(t)} \cdot \frac{P}{RT_p} \cdot (y_{O_2,part\ surf} - y_{O_2,part\ core}) \left[\frac{mol\ O_2}{m^2 \cdot s}\right] \quad (17)$$

where $D_{O2,\ part}$ is the intraparticle oxygen diffusion coefficient, r_p is the particle radius, $y_{O2,\ part\ surf}$ and $y_{O2,\ part\ core}$ are the oxygen volume fractions at the particle surface and at the intraparticle ash/char interface, respectively. $D_{O2,\ part}$ may be calculated from:

$$D_{O_2,part} = \frac{\varepsilon_{part}}{\tau_{part}} D_{O_2,eff} = \frac{1 - y_{Vol} - y_{ash}}{\tau_{part}} D_{O_2,eff} \quad (18)$$

where the char particle porosity, ε_{part}, is calculated by subtraction of the weight fractions of volatiles and ash, y_{Vol} and y_{ash}. The char particle tortuosity for chars is typically around 3 to 5.[45]

The rate of reaction at the unreacted char outer surface between char and oxygen is found from the intrinsic rate expression multiplied with the total moles and divided by the char surface area and product distribution ratio between CO and CO_2:

$$r = \frac{n_C}{A_{char} \cdot \zeta} \cdot k_0 \cdot \exp\left(-\frac{E_a}{RT_p}\right) \cdot y_{O_2,part\ core}^{\ n} \cdot (1-X)^m \left[\frac{mol\ O_2}{m^2 \cdot s}\right] \quad (19)$$

where ζ is the product distribution ratio between CO and CO_2, X is the char fractional conversion degree, and A_{char} is the char surface area. A correlation between temperature and the CO/CO_2 ratio, ζ, during combustion of different coal chars has been reported by Arthur:[46]

$$\zeta = \frac{CO}{CO_2} = 10^{3.4} \cdot \exp\left(-\frac{51916\ J/mol}{R \cdot T}\right) \quad (20)$$

This correlation may be used to estimate ζ at different temperatures under the assumption that it is representative for other chars than coal chars.

At pseudo steady state, the O_2 flux balances the consumption at the char particle surface and the char conversion may be expressed as:

$$\frac{dn_C}{dt} = \zeta \cdot A_{surf} \cdot r \left[\frac{mol\ C}{s}\right] \quad (21)$$

The conversion may also be expressed in terms of fractional conversion, X, instead of moles, n_C, by inserting:

$$X = 1 - \frac{n_C}{n_{C,0}} \quad (22)$$

and

$$dX = \frac{1}{n_{C,0}} dn_C \quad (23)$$

The following expression is then obtained:

$$\frac{dX}{dt} = \frac{\zeta \cdot A_{surf} \cdot r}{n_{C,0}} \quad (24)$$

The unknown oxygen concentrations $y_{O2,surf}$, $y_{O2,part\ surf}$, and $y_{O2,part\ core}$ may be found by solving the four eqs 9, 12, 17, and 19 for the four unknowns r, $y_{O2,surf}$, $y_{O2,part\ surf}$, and $y_{O2,partcore}$. This is easily done for $n = 1$ in eq 19, whereas a numerical solution procedure is required for $n \neq 1$. For $n = 1$, the following expression for char conversion is derived

dx.doi.org/10.1021/ef201353t | Energy Fuels 2012, 26, 854−868

$$\frac{dX}{dt} = \frac{A_{surf}\cdot\zeta}{n_{C,0}}\cdot\frac{y_{O_2,\infty}}{\frac{R\cdot T_g}{k_g\cdot P} + \frac{R\cdot T_b}{P_{AL}\cdot k_{AL}\cdot P} + \frac{r_{p,0}\cdot(1-X)^{1/3}\cdot R\cdot T_p}{D_{O_2,part}\cdot P} + \frac{\zeta\cdot A_{char}}{n_{C,0}\cdot(1-X)^{m+1}\cdot k_0\cdot\exp\left(-\frac{E_a}{R\cdot T_p}\right)}} \quad (25)$$

This expression includes the "resistances" external oxygen transport, oxygen transport into the bed, diffusion into the char particle, and chemical reaction between char and oxygen. The intraparticle diffusion term may be omitted for small char particles or for char particles that rapidly fragment into many smaller char particles. It may also be shown that the term for char oxidation kinetics becomes negligible at high temperatures above 900 °C. Fuel specific, kinetic data, and densities used in the model are summarized in Table 4.

Analysis and Comparison of Char Combustion Model. This section analyses the char combustion model under the experimental conditions in the pilot scale rotary kiln and compares the model predictions with experimental results. The purpose is to study effects of mass, oxygen concentration, bed fill degree, and temperature on the char conversion time.

Table 4. Fuel Specific Data Used in the Char Oxidation Models

fuel property	TDF	pine wood	references
ρ_p [kg/m^3]	1100	690	11
			36
k_0 [1/s]	1.5 (±5.1) · 10^{10}	1.19 · 10^8	18
			47
E_a [kJ/mol]	193 ± 28	140 ± 10	18
			47
exponent m	0.63	0.89	18
			47
LHV [MJ/kg]	37	14	from analysis

Figure 15 left shows the char conversion times for three different pine wood char particles of masses of 0.12 g, 0.24 g, and 0.88 g, respectively. The initial fuel particle dimensions are 30 × 10 × 8 mm, 30 × 10 × 15 mm, and 60 × 30 × 10 mm, respectively. The oxygen concentration is 5% v/v, 10% v/v, or 21% v/v O_2. It is observed that the model, shown with solid lines, predicts a linear relationship between conversion time, char mass, and oxygen concentration. The experimental data also confirm this linear relationship: The conversion time for the 0.88 g char particle is, for example, around 300 s, 600 s, and 1300 s at oxygen concentrations of 21% v/v, 10% v/v, and 5% v/v O_2. The model is generally observed to give a good fit to the experimental data in the experiments with different char masses and oxygen concentrations.

Figure 15 right shows the char conversion time as a function of volumetric bed fill degree and temperature. The fill degrees are 0% (only char in the reactor), 5%, or 10% and the temperatures are 700 °C, 800 °C, 900 °C, or 1000 °C. It is observed that the char conversion time increases when the bed fill degree increases. The model shows the same tendencies in temperature dependence as the experimental results. However, the experimental data show greater differences in conversion time as a function of temperature compared to the model, particularly at 700 °C where the deviation is up to 350 s at 10% fill degree corresponding to a deviation of around 30%.

Figure 16 left shows the char conversion time for three different tire rubber char cylinders with masses of approximately 0.6 g, 1.4 g, and 2.0 g, respectively. The oxygen concentration is 5% v/v, 10% v/v, or 21% v/v O_2. The model, shown with solid lines, predicts a linear increase in conversion time with char mass and a linear decrease with oxygen

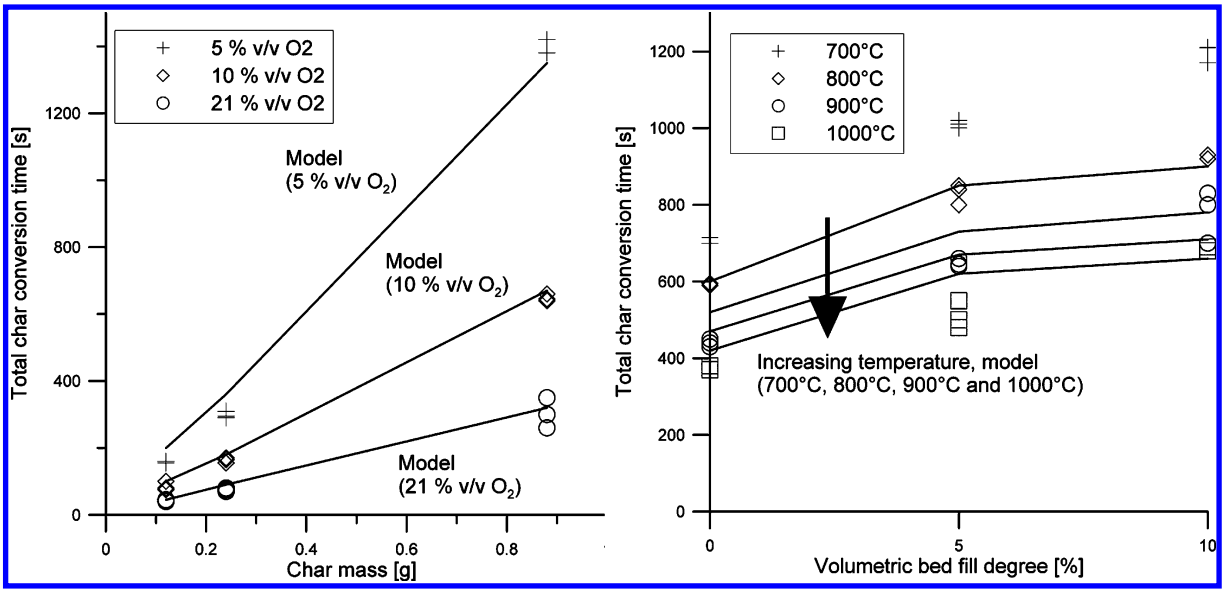

Figure 15. Comparison of experimental data with model predictions for pine wood. Left: Effect of char mass and oxygen concentration on the char conversion time. 900 °C, 5% fill degree, 100 NL/min. Initial particle dimensions: 30 × 10 × 8 mm, 30 × 10 × 15 mm and 60 × 30 × 10 mm. Right: Effect of raw material fill degree and temperature on model predicted char conversion time for a pine wood char particle with initial dimensions of 60 × 30 × 10 mm. Char mass = 0.88 g. 10 % v/v O_2, 100 NL/min. Char conversion evaluated at 80% conversion degree.[18]

dx.doi.org/10.1021/ef201353t | Energy Fuels 2012, 26, 854–868

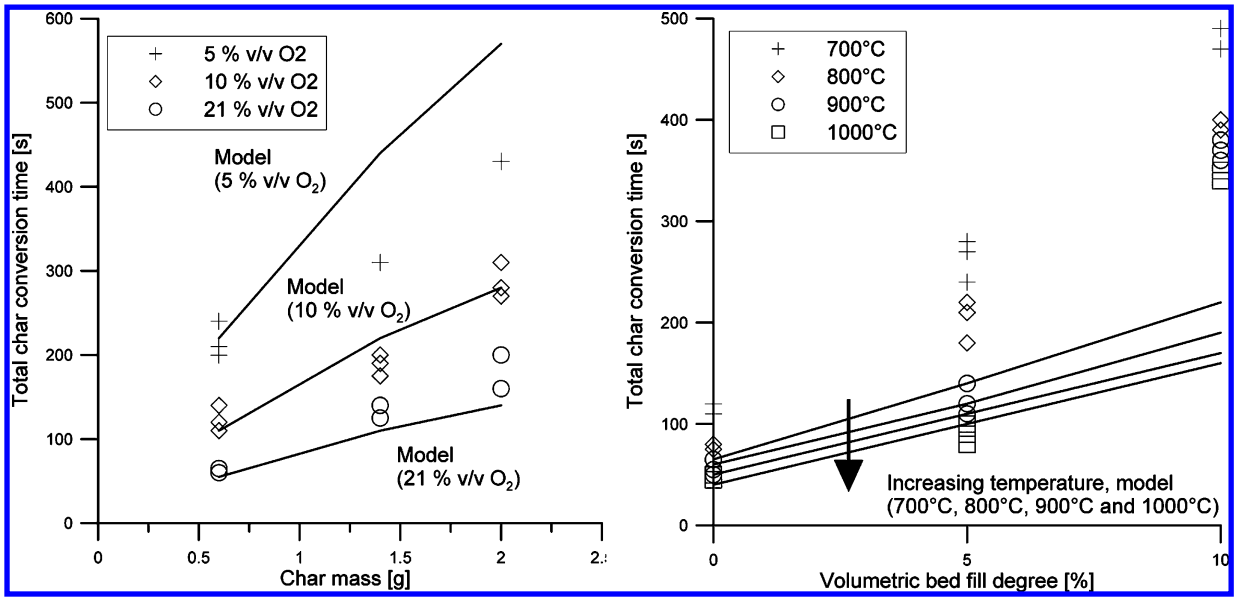

Figure 16. Left: Comparison between model predictions and experimental data for char conversion time of three different tire rubber char cylinders with lengths of 25 mm and initial diameters of 9 mm, 12 mm, and 16 mm, respectively. 900 °C, 5% raw material fill, 100 NL/min. Char masses and oxygen concentrations indicated on figure. Right: Effect of raw material fill degree and temperature on model predicted char conversion time for tire char cylinder with a length of 25 mm and initial diameter of 9 mm. Char mass = 0.6 g. 10 % v/v O_2, 100 NL/min. Char conversion evaluated at 80% conversion degree.[18]

concentration. For example, the predicted conversion time for 2 g of char is observed to be halved from 570 to 280 s when the oxygen concentration is doubled from 5% v/v to 10% v/v. Thus, the model predicts that external mass transfer of oxygen from gas to fuel particle is a main rate limiting parameter. The model gives the best agreement with the experimental values at 10% v/v and 21% v/v O_2, where the deviation is generally within ±50 s, but the model fails to give good agreement with the experiments at 5% v/v O_2 and char masses of 1.4 g and 2.0 g. In these cases, the deviations are up to nearly 30%.

Figure 16 right shows the predicted effect of raw material fill degree in the interval of 0−10% and in the temperature interval of 700−1000 °C for a cylindrical tire rubber char particle. Experimental values are also compared with the model. Both experimental values and the model show that the char conversion time increases with volumetric bed fill degree and decreases when the temperature increases. The model only fits the experimental values in the case with a fill degree of 0%, corresponding to a situation with only char in the pilot scale rotary kiln and no cement raw materials. However, the experimental values at 700 °C and 0% fill show longer conversion times than predicted by the model: 120−130 s relative to 65 s, respectively. At 5% fill degree, the model only fits the experimental values at 900 °C and 1000 °C but underestimates the conversion times at 700 °C and 800 °C by a factor of 2, and at a fill degree of 10%, the model underestimates the effect of fill degree and temperature by a factor of 2.5 to 3, depending on temperature. The effect of fill degree seems to increase more with fill degree for tire rubber than for pine wood. The reason for these differences may be related to the chemical and physical properties of the different chars: Tire char fragments into several small particles while the wood char to a high degree retains its size and shape.

Conclusions on Char Conversion Model. A model for char conversion has been suggested and compared with experimental data for large particles of tire char and pine wood char. The model includes the four resistances: external oxygen diffusion to raw material bed, oxygen transport into the bed, intraparticle oxygen diffusion, and chemical reaction at the char surface.

The model is in good correspondence with the observed conversion times for pine wood char. However, it underestimates the effect of bed fill degree for tire char. The model also underestimates the effect of the lowest temperatures of 700 °C and 800 °C on the conversion time for both pine wood char and tire char. Regarding the effect of material fill degree on the char conversion time, it is required to make more experiments with different fuel chars and particle sizes/shapes to obtain a better basis for model validation.

■ CONCLUSIONS

Experiments with tire rubber and pine wood in a high temperature pilot scale rotary kiln have been conducted in order to quantify the effect of key process parameters such as bed fill degree, kiln rotational speed, temperature, etc. on the fuel conversion time. The process conditions have been chosen to simulate the process conditions in the material inlet end of a modern cement rotary kiln. Investigated temperatures varied from 700 °C to 1000 °C, oxygen concentrations varied from 5% v/v O_2 to 21% v/v O_2, volumetric raw material bed fill degrees varied from 0% to 10%, and kiln rotational speeds varied from 3 rpm to 20 rpm.

The results showed that devolatilization of tire rubber and pine wood was mainly influenced by the temperature and fuel particle size. The devolatilization times were from 40 s for a 10 mm diameter tire rubber particle at 1000 °C to 170 s for a 20 mm diameter pine wood particle at 700 °C. The char oxidation was influenced by all investigated parameters fuel sample mass, particle size, temperature, oxygen concentration, bed fill degree, and rotational speed. Rotational speed, however, was only of importance if there was a shift in bed motion, e.g., from slumping to rolling. For changes in rotational speed where the

dx.doi.org/10.1021/ef201353t | Energy Fuels 2012, 26, 854−868

dominant bed motion was maintained as the rolling motion, the effect of rotational speed was of minor importance.

The tire char was observed to fragment into smaller particles during the char oxidation, leading to shorter conversion times than for pine wood char which predominantly behaved as one shrinking particle during the char oxidation. The found char conversion times were from 40 s to 480 s for tire char and from 30 s to 1300 s for pine wood char, depending on the conditions.

Devolatilization and char oxidation models have been developed and compared with experimental results and published data. These models may be further modified to predict fuel conversion times in industrial cement rotary kilns.

AUTHOR INFORMATION

Corresponding Author

*E-mail: arni@flsmidth.com. Telephone: +45 36181970.

ACKNOWLEDGMENTS

The work described in this Article is part of a research platform on future cement technology financed by The Danish National Advanced Technology Foundation, Technical University of Denmark (DTU), and FLSmidth A/S.

NOMENCLATURE

A = Surface area (m^2)
Bi = Biot number (-)
C_p = Specific heat capacity (J/(kg·K))
D = Diameter (mm or m)
D_{O2} = Diffusion coefficient (m^2/s)
E_a = Activation energy (J/mol)
F = Fill degree (-)
FC = Fixed Carbon (wt %)
Fr = Froude number (-)
h = Heat transfer coefficient ($W/(m^2K)$)
k = Mass transfer coefficient (m/s)
k_p = Thermal conductivity (W/(m·K))
k_0 = Pre-exponential factor (1/s)
L = Length (m)
LHV = Lower Heating Value (MJ/kg)
n = Moles (Mole)
P = Pressure (Pa) or probability (%)
r = Radius (mm or m) or rate (mol/m^2s)
R = Universal gas constant (J/(mol·K)
Sc = Schmidt number (-)
Sh = Sherwood number (-)
t = Time (s or min)
T = Temperature (°C or K)
Y = Distribution between bed and gas (-)
X = Degree of conversion (-)
V = Volume (m^3)
VM = Volatile Matter (wt %)
α = Thermal diffusivity (m^2/s)
β = Positive solutions (-)
ε = Emissivity or Porosity (-)
σ = Stefan–Boltzmanns constant ($5.72 \cdot 10^{-8}$ $W/(m^2K^4)$)
ρ = Density (kg/m^3)
τ = Tortuosity (-)
ζ = CO/CO_2 distribution ratio (-)
ω = Rotational speed (min^{-1})

Subscripts

a = Average
AL = Active Layer
b = Bed
cond = Conduction
conv = Convection
eff = Effective
g = Gas
p = Particle
part = Particle surface
rad = Radiation
sph = Spherical
surf = Surface
Vol = Volatile
w = Wall
∞ = Surroundings

REFERENCES

(1) VDZ, *Activity Report 2007–2009*; 2009, http://www.vdz-online.de. Obtained April 20, 2011.
(2) Cembureau, *Activity Report 2008*; http://www.cembureau.be. Obtained April 20, 2011.
(3) *BP Statistical Review of World Energy*; June 2009, http://www.bp.com. Obtained April 20, 2011.
(4) Cembureau, *Alternative Fuels in Cement Manufacture*; 1997, http://www.cembureau.be. Obtained April 20, 2011.
(5) Nielsen, A. R.; Larsen, M. B.; Glarborg, P.; Dam-Johansen, K. *Energy Fuels* **2011**, *25*, 2917–2926.
(6) Bouvier, J. M.; Charbel, F.; Gelus, M. *Resour. Conserv.* **1987**, *15*, 205–214.
(7) Yang, J.; Tanguy, P. A.; Roy, C. *AIChE J.* **1995**, *41* (6), 1500–1512.
(8) Yang, J.; Tanguy, P. A.; Roy, C. *Chem. Eng. Sci.* **1995**, *50* (12), 1909–1922.
(9) Schmidthals, H. *Luftvergasung von Altreifen zur integrierten stofflichen und energetischen Nutzung im Klinkerbrennprozess*; Doktor-Ingenieur Dissertation, Fakultät für Maschinenbau, Ruhr-Universität Bochum, Germany, 2001.
(10) Giddings, D.; Pickering, S. J.; Simmons, K.; Eastwick, C. N. *J. Energy Inst.* **2002**, *75*, 91–99.
(11) Larsen, M. B.; Schultz, L.; Glarborg, P.; Skaarup-Jensen, L.; Dam-Johansen, K.; Frandsen, F.; Henriksen, U. *Fuel* **2006**, *85*, 1335–1345.
(12) Chinyama, M. P. M; Lockwood, F. C. *J. Energy Inst.* **2007**, *80* (3), 162–167.
(13) Conesa, J. A.; Font, R.; Fullana, A.; Caballero, J. A. *Fuel* **1998**, *77* (13), 1469–1475.
(14) Leung, D. Y. C; Wang, C. L. *J. Anal. Appl. Pyrolysis* **1998**, *45*, 153–169.
(15) Kyari, M.; Cuncliffe, A.; Williams, P. T. *Energy Fuels* **2005**, *19*, 1165–1173.
(16) Atal, A.; Levendis, Y. A. *Fuel* **1995**, *74* (11), 1570–1581.
(17) Masi, S.; Salatino, S.; Senneca, O. *Fluidised Bed Combust.* **1997**, *1*, 135–143.
(18) Larsen, M. B.; Hansen, M. L.; Glarborg, P.; Skaarup-Jensen, L.; Dam-Johansen, K.; Frandsen, F. *Fuel* **2007**, *86*, 2343–2350.
(19) Winter, F.; Prah, M. E.; Hofbauer, H. *Combust. Flame* **1997**, *108*, 302–314.
(20) Di Blasi, C. *Chem. Eng. Sci.* **2000**, *55*, 5999–6013.
(21) De Diego, L. F.; García-Labiano, F.; Gayán, P; Abad, A.; Adánez, J. *J. Anal. Appl. Pyrolysis* **2002**, *65*, 173–184.
(22) De Diego, L. F.; García-Labiano, F.; Gayán, P; Abad, A; Adánez, J. *Ind. Eng. Chem. Res.* **2002**, *41*, 3642–3650.
(23) Di Blasi, C.; Branca, C. *Energy Fuels* **2003**, *17*, 247–254.
(24) Jand, N.; Foscolo, P. U. *Ind. Eng. Chem. Res.* **2005**, *44*, 5079–5089.
(25) Janse, A. M. C.; de Jonge, H. G.; Prins, W.; van Swaaij, W. P. M *Ind. Eng. Chem. Res.* **1998**, *37*, 3909–3918.
(26) Senneca, O. *Fuel Proc. Technol.* **2007**, *88*, 87–97.
(27) Shen, D. K.; Gu., S.; Luo, K. H.; Bridgwater, A. V.; Fang, M. X. *Fuel* **2009**, *88*, 1024–1030.

(28) Tans, P.; Keeling, R. *Trends in Atmospheric Carbon Dioxide*; NOAA/ESRL, www.esrl.noaa.gov/gmd/ccgg/trends/. Obtained December 9, 2011.
(29) Larsen, M. O.; Hellesen, B.; *Statistik 1*, 3rd ed.; Institute of Applied Chemistry, Technical University of Denmark, Lyngby, Denmark, 1998 (in Danish).
(30) Jensen, A. *Heating and devolatilization of coal particles*; Course note, Department of Chemical Engineering, Technical University of Denmark, Lyngby, Denmark, 1997.
(31) Agarwal, P. K.; Genetti, W. E.; Lee, Y. Y. *Chem. Eng. Sci.* **1986**, *41* (9), 2373−2383.
(32) Szekely, J.; Ewans, J. W.; Sohn, H. Y. *Gas-solid reactions*; New York: Academic Press, 1976; Vol. *51*.
(33) Agarwal, P. K.; Genetti, W. E.; Lee, Y. Y. *Fuel* **1984**, *63*, 1748−1752.
(34) Kim, S.-S.; Kim, J.; Park, Y.-H; Park, Y.-K. *Bioresour. Technol.* **2010**, *101*, 9797−9802.
(35) Kunii, D.; Levenspiel, O. *Fluidization Engineering*, 2nd ed.; Butterworths: Boston, MA, USA, 1991; ISBN: 0-409-90233-0.
(36) Leon, G.; Cruz-de-Leon, J.; Villasenor, L. *Holz als Roh- und Werkstoff* **2000**, *58*, 241−246.
(37) Sellassie, K. G.; Moo-Young, H. K.; Lioyd, T. B. *Int. J. Environ. Waste Manage.* **2007**, *1* (2/3), 179−191.
(38) Linjewile, T. M.; Hull, A. S.; Agarwal, P. K. *Chem. Eng. Sci.* **1993**, *48* (21), 3671−3675.
(39) Tscheng, S. H.; Watkinson, A. P. *Can. J. Chem. Eng.* **1979**, *57*, 433−443.
(40) Nielsen, A. R.; Aniol, R. W.; Larsen, M. B.; Glarborg, P.; Dam-Johansen, K. *Powder Technol.* **2011**, *210*, 273−280.
(41) Larsen, M. B. Alternative fuels in Cement Production. Ph.D. Thesis, Department of Chemical Engineering, Technical University of Denmark, Lyngby, Denmark, 2007; ISBN: 978-87-91435-49-8.
(42) Green, D. W.; Perry, R. H. *Perry's Chemical Engineers' Handbook*, 8th ed., McGraw-Hill: China, 2008; ISBN: 978-0-07-142294-9.
(43) Heydenrych, M. D. *Modelling of rotary kilns*. PhD Thesis, University of Twente, The Netherlands, 2001; ISBN: 90-36515440.
(44) Dias, R.; Teixeira, J. A.; Mota, M.; Yelshin, A. *Sep. Purif. Technol.* **2006**, *51*, 180−184.
(45) Johnsson, J. E.; Jensen, A. *Proc. Combust. Inst.* **2000**, *28*, 2353−2359.
(46) Arthur, J. R. *Trans. Faraday Soc.* **1951**, *47* (2), 164−178.
(47) Kastanaki, E.; Vamvuka, D. *Fuel* **2006**, *85*, 1186−1193.